

HVIS2022-RXGKQWQLXN

FLUID-SOLID COUPLED SIMULATION OF HYPERVELOCITY IMPACT AND PLASMA FORMATION

Shafquat T. Islam¹, Wentao Ma¹, John G. Michopoulos², Kevin G. Wang^{1,*}

¹Department of Aerospace and Ocean Engineering, Virginia Tech, 460 Old Turner St, Blacksburg, VA 24061, USA

²U.S. Naval Research Laboratory, 4555 Overlook Ave., SW, Washington, DC 20375, USA

ABSTRACT

Previous computational studies on hypervelocity impact have largely focused on predicting the dynamic response of the solid materials that constitute the projectile and the target, while the surrounding environment is often assumed to be a vacuum. In this paper, we present a computational model that includes the dynamics, thermodynamics, and ionization of the surrounding fluid material. The model couples the compressible inviscid Navier-Stokes equations with the Saha ionization equations. The three material interfaces between the projectile, the target, and the ambient fluid are tracked implicitly by solving two level set equations that share the same velocity field. Across material interfaces, the mass, momentum, and energy fluxes are computed using the FInite Volume method with Exact multi-material Riemann problems (FIVER), which accounts for the discontinuity of both state variables and the equation of state. The computational model is applied to a specific case involving a tantalum rod projectile impacting onto a soda lime glass target in an argon gas environment. The impact velocity is varied between 3 km/s and 6 km/s in different simulations. The velocity and thermodynamic state within the solid materials are compared with their counterparts in the surrounding gas. The result reveals a region of argon gas with high pressure and temperature, formed in the early stage of the impact mainly due to the hypersonic compression of the fluid between the projectile and the target. The temperature within this region is significantly higher than that in the solid materials. For impact velocities higher than 4 km/s, ionization is predicted in this region.

NOMENCLATURE

c	Molar fraction
c_0	Bulk speed of sound under ambient condition, dimension: $[L t^{-1}]$
c_p	Specific heat capacity $[L^2 t^{-2} T^{-1}]$
e	Specific internal energy $[L^2 t^{-2}]$
e_t	Specific total energy $[L^2 t^{-2}]$
η	Volumetric strain

g	Electron degeneracy
Γ_0	Grüneisen parameter at reference (ambient) condition
γ	Thermodynamic constant
I	Ionization energy $[M L^2 t^{-2}]$
J	Number of elemental species in plasma mixture
l	Angular momentum quantum number
n	Number density of a (charged) species $[L^{-3}]$
n_e	Plasma density $[L^{-3}]$
n_H	Number density of nuclei $[L^{-3}]$
Ω	Computational domain
p	Pressure $[M L^{-1} t^{-2}]$
p_c	Thermodynamic constant for stiffened gas $[M L^2 t^{-2}]$
r	Charge of a species $[I t^{-1}]$
ρ	Density $[M L^{-3}]$
s	Slope of Hugoniot curve
T	Temperature $[T]$
U	State dependent partition function
u_s	Shock velocity $[L t^{-1}]$
u_p	Particle velocity $[L t^{-1}]$
Z	Atomic number
Z_{av}	Mean charge $[I t^{-1}]$

Subscripts

n	electronic energy level
r	ionic charge state

Constants

ϵ_0	permittivity of free space $[8.85 \times 10^{-12} m^{-3} kg^{-1} s^4 A^2]$
h	Planck's constant $[6.62 \times 10^{-34} m^2 kg s^{-1}]$
k_b	Boltzmann's constant $[1.38 \times 10^{-23} m^2 kg s^{-2} K^{-1}]$
m_e	stationary mass of an electron $[9.11 \times 10^{-33} kg]$

1. INTRODUCTION

Hypervelocity impact is a challenging multiphysics problem that features the rapid transport and dissipation of kinetic energy through mechanical, thermal, chemical, and electromagnetic pathways. In the past, extensive research has been conducted to understand and predict the mechanical response of the target and the projectile, such as shock waves, large deformation, fracture, and fragmentation [1–4]. It has also been shown that

*Corresponding author: kevinw3@vt.edu

the temperature behind the shock waves can exceed thousands of Kelvin, causing the solid materials to ionize, thereby forming a plasma [5, 6]. One of the earliest reports of impact-generated plasma was by Friichtenicht and Slattery (1963) [7], in which spherical projectiles made of iron and graphite were accelerated using an electrostatic accelerator to velocities of up to 16 km/s. Since then, various authors have published data that characterize the composition and energy of plasma generated under different impact conditions (e.g., [8–10]). In the past decade, there has been growing interest in developing computational models to predict impact-generated plasma and electromagnetic waves. For example, Li *et al.* [11, 12] simulated hypervelocity impact of aluminum projectile and target for impact velocities between 5 and 10 km/s using both commercial and self-developed codes that couple smooth particle hydrodynamics (SPH) with the Thomas-Fermi model. Fletcher *et al.* [10] also developed a SPH code to simulate hypervelocity impacts and used the non-ideal Saha equations to predict ionization in the target material. Later, Fletcher *et al.* developed a particle-in-cell (PIC) code to investigate the source of electromagnetic emission from the impact generated plasma [13]. Despite these progresses, the generation of plasma and electromagnetic waves from hypervelocity impacts remains an active research area. Open questions in this area include the source (i.e. projectile, target, or the surrounding gas) and composition of plasma, the dependence of plasma energy on impact velocity (cf. [8, 9]), and the energy and spectrum of the electromagnetic emissions [13].

Previous theoretical and computational studies on hypervelocity impact have largely focused on the dynamic response and material behaviors of the projectile and the target, while the ambient environment is usually assumed to be a vacuum. This assumption is often valid when studying collisions that occur in the exoatmospheric space environment. Nonetheless, for terrestrial and atmospheric applications in which the collision occurs in a fluid — more specifically, gas — medium, the projectile produces a shock-dominated hypersonic fluid flow during its flight, which can easily exceed Mach 10. The impact leads to the emission of another strong shock wave in the fluid that disrupts the initial flow. Compared to the solid materials that constitute the projectile and the target, the ambient gas has much lower density, and is far more compressible. The gaseous material behind the shock wave may also reach a high temperature, possibly higher than that in the solids. Therefore, the ambient gas may also ionize, and contribute to the plasma mixture formed during hypervelocity impact events. Understanding the fluid dynamics, thermodynamics, and plasma characteristics is important for developing a complete description of hypervelocity impacts that occur in a fluid medium. The knowledge obtained may also lead to the development of new diagnostic tools for impact detection and characterization.

In this paper, we present the development of a fluid-solid coupled computational model of hypervelocity impact, including the formation of plasma within the ambient fluid. The model combines the compressible inviscid Navier-Stokes equations with the Saha ionization equations. We solve the Navier-Stokes equations in the Eulerian reference frame using a high-resolution finite volume method. The spatial domain includes three subdomains, occupied by the projectile, the target, and the surrounding fluid,

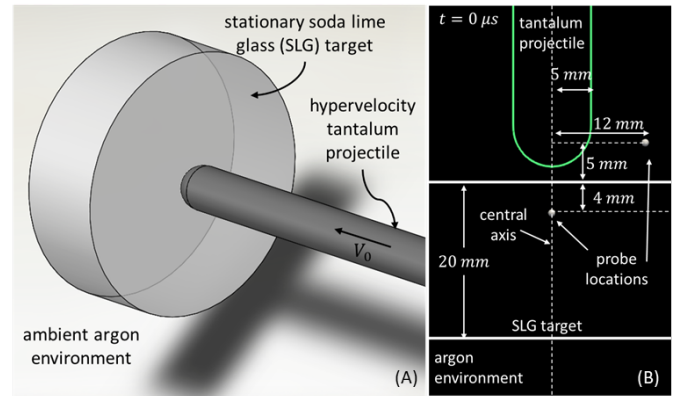


FIGURE 1: PROBLEM SETUP. (A) A 3D DEPICTION OF THE TARGET, PROJECTILE, AND AMBIENT FLUID IN THE MODEL PROBLEM. (B) A 2D CROSS-SECTION WITH ANNOTATED GEOMETRY AND PROBE LOCATIONS.

respectively. The boundaries of the projectile and the target are represented implicitly as the 0 level set of two signed distance functions. Across the material interfaces between the subdomains, mass density differs by several orders of magnitude and the thermodynamic relations (i.e. equations of state) also differ significantly. These types of discontinuities pose a challenge to the computation of fluxes across material interfaces. In this work, we compute the mass, momentum, and energy fluxes across material interfaces using the Finite Volume method based on Exact multi-material Riemann problem (FIVER) [14–16]. By constructing and solving an exact bimaterial Riemann problem along each edge in the mesh that crosses a material interface, FIVER explicitly accounts for the change of equation of state across the interface. Previously, FIVER has been validated for several shock-dominated multiphase flow and fluid-structure interaction problems in underwater explosion and implosion, pipeline explosion, cavitation erosion, and shock wave lithotripsy [15, 17–22]. Within the fluid subdomain, we solve the Saha equations to predict the onset of ionization and the distribution of ionization products. This model assumes local thermodynamic equilibrium, which can be justified for predicting the formation and initial expansion of plasma during hypervelocity impacts [10, 23].

We apply the computational model to simulate the impact of a tantalum rod projectile onto a target made of soda lime glass (SLG) in an argon gas environment (Fig. 1). Tantalum is a hard, refractory metal that is often used in impact experiments and applications. SLG is selected as the target material for its potential application in armor and protective systems [24]. It is inexpensive, transparent, and has relatively high mechanical strength. Argon is selected as the ambient fluid because it is monoatomic, and chemically inert even under extreme pressure and temperature conditions. The projectile’s impact velocity, denoted by V_0 in this paper, is varied between 3 km/s and 6 km/s in different simulations. The velocity and thermodynamic state within the solid and fluid materials are investigated and compared. The extent of ionization in the ambient fluid is characterized by the mean charge.

2. MATERIALS AND METHODS

2.1 Continuum dynamics

Figure 1 presents the setup of the hypervelocity impact problem investigated in this paper. The projectile is a cylindrical tantalum rod of 5 mm radius, with a semi-spherical leading edge. The target is a cylindrical plate made of SLG with a radius of 30 mm and a height of 20 mm. In the far-field, the density, pressure, and temperature of argon are fixed at 1.78 kg/m³, 100 kPa, and 300 K, respectively. Figure 1(B) displays the geometry of the three material subdomains and the location of two virtual probes that are placed within the SLG target and the ambient gas, respectively.

Because of the high impact velocities, the solid materials involved in this problem, namely tantalum and SLG, are modeled as compressible fluids. When the impact velocity exceeds 3 km/s, the density of the energy transferred from the projectile to the SLG target is far greater than the strain energy density of SLG. In the past, Kobayashi *et al.* showed that when impacted by steel and tungsten projectiles traveling at 4 km/s to 6 km/s, the maximum pressure inside SLG exceeds 50 GPa [6], which is an order of magnitude higher than the material's Hugoniot elastic limit (3 GPa to 8 GPa). Tantalum also has a relatively low Hugoniot elastic limit, around 2 GPa [25].

Therefore, the dynamics of the target, the projectile, and the surrounding gas can be considered to be governed by the three-dimensional (3D) compressible Navier-Stokes equations. In addition, we neglect the effects of viscosity and heat diffusion, which reduces the Navier-Stokes equations to

$$\frac{\partial}{\partial t} \begin{bmatrix} \rho \\ \rho V \\ \rho e_t \end{bmatrix} + \nabla \cdot \begin{bmatrix} \rho V^T \\ \rho V \otimes V + p\mathbf{I} \\ (\rho e_t + p)V^T \end{bmatrix} = 0, \quad (1)$$

also known as the Euler equations. Here ρ , V , e_t , p denote density, velocity, specific total energy, and pressure, respectively. \mathbf{I} is the 3D identity matrix.

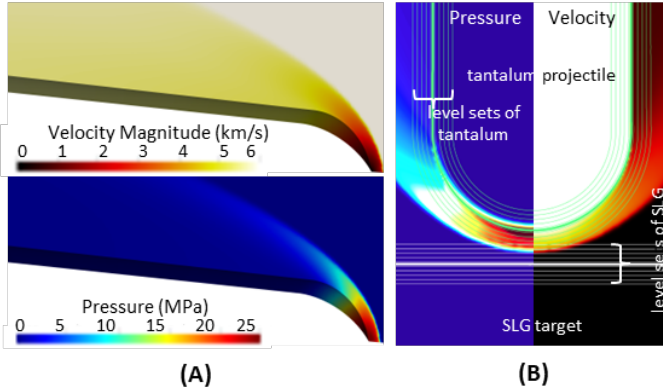


FIGURE 2: (A) PRESSURE AND VELOCITY FIELDS OF ARGON GAS FLOW AROUND THE LEADING EDGE OF THE PROJECTILE. (B) INITIAL CONDITION OF THE IMPACT ANALYSIS.

Each simulation is performed in two steps, namely a steady-state computational fluid dynamics (CFD) analysis, followed by a fluid-solid coupled impact analysis. In both steps, the Navier-Stokes equations (Eq. (1)) are solved using a high-resolution finite

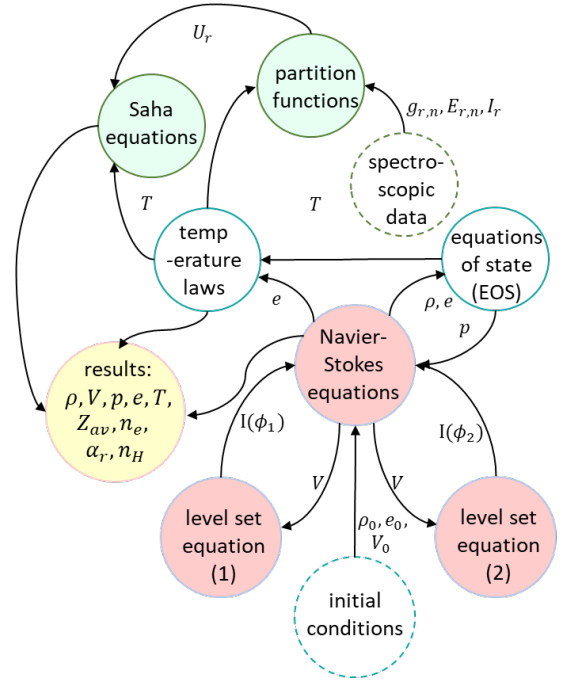


FIGURE 3: OVERVIEW OF THE COMPUTATIONAL MODEL.

volume method. The steady-state CFD analysis is performed using the AERO-F solver [26] on an unstructured, body-fitted mesh. In the most refined region, the characteristic element size is approximately 0.15 mm. This analysis is used to obtain the flow around the projectile in-flight at a hypersonic velocity. The body (i.e. projectile) stationary reference frame is adopted, and the impact velocity is prescribed by means of far-field boundary condition. In particular, this analysis captures the curved bow shock, as shown in Fig. 2(A). The pressure, velocity, and density of this 3D analysis are extracted and mapped on to a non-body-fitted Cartesian mesh after converting the reference frame to be ground stationary. In the most refined region, the element size is 0.1 mm. The fluid-solid coupled impact analysis is performed on this mesh using the M2C solver [27]. The results of this analysis is discussed in details in Sec. 3. The two solvers used in this study, namely AERO-F [26] and M2C [27], are both publicly available. The schematic of the computational framework adopted in this study is summarized in Fig. 3.

2.2 Material models

Equation (1) is algebraically closed by a thermodynamic equation of state (EOS) for each material. In this work, tantalum is modeled using the Mie-Grüneisen EOS [32], in the form of

$$p(\rho, e) = \frac{\rho_0 c_0^2 \eta}{(1 - s\eta)^2} \left(1 - \frac{1}{2} \Gamma_0 \eta\right) + \rho_0 \Gamma_0 e, \quad (2)$$

where e is the specific internal energy, and ρ_0 and c_0 denote the density and bulk speed of sound in the ambient condition. s is the slope of the Hugoniot curve. Γ_0 is the Grüneisen parameter. η is the volumetric strain, and can be expressed as: $1 - \rho_0/\rho$. Argon is modeled using the perfect gas EOS, with specific heat ratio $\gamma = 1.667$. The SLG target is modeled using the stiffened

Substance	EOS	Parameters				
Tantalum	Mie-Grüneisen	c_0 (km/s)	s	ρ_0 (g/cm ³)	Γ_0	c_v (J/(K · kg))
		3.293 [28]	1.307 [28]	16.65 [29]	1.64 [30]	139
Soda lime glass (SLG)	Stiffened gas	γ	p_c (GPa)	c_v (J/(K · kg))		
		3.9	2.62	1156 [31]		
Argon	Perfect gas	γ	c_v (J/(K · kg))			
		1.667	312.2			

TABLE 1: PARAMETERS OF THE EQUATIONS OF STATE

gas EOS [33], i.e.

$$p(\rho, e) = (\gamma - 1)\rho e - \gamma p_c, \quad (3)$$

where γ and p_c are empirical model parameters.

SLG is modeled after the glass commercially known as Starphire[®], which has a chemical composition (by weight): 73% SiO₂, 14% Na₂O, 10% CaO, and 3% MgO [34]. Unlike tantalum, SLG is not modeled using the Mie-Grüneisen EOS, because certain regions in the SLG target experience high tensile stresses during hypervelocity impact, while the Mie-Grüneisen EOS has been primarily used to model materials in compression [32]. On the other hand, the stiffened gas EOS can be calibrated to capture the shock Hugoniot obtained from laboratory experiments [33]. Specifically, we combine Eq. (3) with the Rankine-Hugoniot jump conditions, then fit them to the shock Hugoniot, $u_s = c_0 + su_p$, obtained from laboratory impact experiments, where u_s and u_p denote the shock speed and the downstream particle velocity, respectively. The shock Hugoniot data presented in [35] ($c_0 = 2.01$ km/s, $s = 1.7$) is adopted in this work, which gives $\gamma = 3.9$ and $p_c = 2.62$ GPa.

For all the materials, temperature is assumed to be a function of only specific internal energy (e). A constant specific heat is specified for each material, which yields a linear relation, $T = (e - e_0)/c_v + T_0$, where T denotes temperature and the subscript 0 refers to a reference state. The monoatomic configuration and the absence of valence electrons entail that argon atoms have only translational degrees of freedom, but not vibrational, rotational, or electronic degrees of freedom. Therefore, the specific heat of argon is independent of temperature, which justifies the use of a constant specific heat. For the solid materials, the specific heat is computed using the Dulong-Petit law, which matches reasonably well with measurements obtained in laboratory experiments. All the material parameters used in the simulations are presented in Table 1.

2.3 Interface tracking and treatment

At any time $t \geq 0$, the physical domain Ω consists of three material subdomains, occupied by argon, tantalum, and SLG, respectively. Across material interfaces, pressure and the normal component of velocity are continuous, whereas density and the tangential components of velocity are generally discontinuous. During a hypervelocity impact event, the material subdomains undergo rapid deformation. As such, the motion of the material interfaces are predicted by solving two level set equations that

share the common velocity field [36]. This method allows us to keep track of three sharp, interconnected material interfaces (i.e. projectile-fluid, target-fluid, and projectile-target) that undergo large, complex deformations. Specifically, two level set equations of the form

$$\frac{\partial \phi_s}{\partial t} + V \cdot \nabla \phi_s = 0, \quad s = 1, 2 \quad (4)$$

are solved synchronously to track the boundaries of the copper projectile and the SLG target, respectively. The two level set functions, ϕ_1 and ϕ_2 , are initialized to be the signed distance from each point in the computational domain to the surface of the target and the projectile, respectively. Notably, the two level set equations share the same velocity field. As a result, the contact and separation between the projectile and the target are captured naturally, while spurious overlaps are avoided. The mass, momentum, and energy fluxes across material interfaces are computed using the method of FIVER (FInite Volume method based on Exact multiphase Riemann solvers), which has been validated for several multiphase flow problems featuring large density jumps [15, 20, 22]. Following this method, a one-dimensional bimaterial Riemann problem is constructed along each edge in the mesh that crosses a material interface. The solution of this exact Riemann problem is used to compute the local fluxes.

2.4 Ionization model

The plasma density, molar fraction of each ionic state, and average charge of the plasma are calculated by solving the Saha equations, i.e.

$$\frac{n_{r+1}n_e}{n_r} = 2 \frac{U_{r+1}}{U_r} \left[\frac{2\pi m_e k_B T}{h^2} \right]^{3/2} \exp\left(\frac{-I_r}{k_B T}\right), \quad r = 0, 1, \dots, N, \quad (5)$$

where n_r is the number density of the r -th charge state ion, n_e is the number density of electrons (also referred to as the plasma density), T is the temperature, h is the Planck constant, k_B is the Boltzmann constant, m_e is the stationary mass of an electron, and I_r the r -th ionization energy. $N = Z - 1$ where Z is the atomic number (18 for argon).

This equation assumes the condition of local thermodynamic equilibrium. A plasma under this condition must also obey the condition of quasi-neutrality (i.e. conservation of charge), and from conservation of mass also follows that the plasma must observe conservation of nuclei. Following the discussion of Zaghoul *et al.* [37], the combination of these conservation laws with

equation (5) yields the one-dimensional transcendental equation,

$$Z_{\text{av}} \left(1 + \sum_{r=1}^N \frac{\prod_{m=1}^r f_m}{(Z_{\text{av}} n_H)^r} \right) = \sum_{r=1}^N \left(\frac{r}{(Z_{\text{av}} n_H)^r} \prod_{m=1}^r f_m \right), \quad (6)$$

where Z_{av} denotes the average charge number of neon, and n_H the number density of heavy particles. f_m is given by

$$f_m = 2 \frac{U_{m+1}}{U_m} \left(\frac{2\pi m_e k_B T}{h^2} \right)^{\frac{3}{2}} \exp \left(- \frac{I_m}{k_B T} \right). \quad (7)$$

U_r is the state-dependent partition function of the r -th charge state ion, given by

$$U_r = \sum_{n=1}^{n_{\text{max}}} g_{r,n} \exp \left(- \frac{E_{r,n}}{k_B T} \right), \quad (8)$$

where $g_{r,n}$ and $E_{r,n}$ denote the degeneracy and excitation energy of the r -th ion at the n -th energy level. The statistical weighting is done by the degeneracy, $g_{r,n}$ and is related to the angular momentum quantum number, $l_{r,n}$, via the following relation,

$$g_{r,n} = 2l_{r,n} + 1 \quad (9)$$

The summation in (8) is limited to a maximum excitation state at $n = n_{\text{max}}$, where n_{max} indicates the last element in the $E_{r,n}$ sequence ($n = 1, 2, \dots$) that is smaller than or equal to I_r . The values of I_r , $E_{r,n}$, and $l_{r,n}$ for all elements modelled in this study are obtained from the NIST atomic spectral database [38].

In each time step, we solve Eq. (6) for Z_{av} using a safeguarded iterative method, TOMS748 [39], at each node within the subdomain occupied by argon. After that, the plasma density and molar fraction of each ion state can be easily calculated following the method described by Zaghoul *et al.* [37]. To accelerate the solution process, we tabulate U_r , $r = 0, 1, \dots, 10$ as functions of $\exp(-1/T)$ at the beginning of the impact analysis. In each time step, we calculate the values of U_r using cubic spline interpolation.

3. RESULTS AND DISCUSSION

Our primary discussion of results follows a representative case with impact velocity $V_0 = 5$ km/s. In the impact analysis, the projectile is initialized to be 2 mm away from the target. Therefore, impact occurs at time $t = 0.4 \mu\text{s}$. A sequence of snapshots of the simulation results are shown in Fig. 4. The columns in this image (from left to right) represent the pressure, velocity magnitude, temperature, and average charge fields. Since the temperature and average charge fields span several orders of magnitude, they have both been plotted on a logarithmic scale. Each row of images represent the states at progressive time instances of (from top to bottom) $t = 0.625 \mu\text{s}$, $1.25 \mu\text{s}$, $2.5 \mu\text{s}$, and $5 \mu\text{s}$.

The sudden deceleration of the projectile due to the impact imparts a large amount of energy from the projectile into the target and the surrounding fluid. This decelerated region can be seen in the velocity field plot at $t = 0.625 \mu\text{s}$. The impact also causes the formation of high pressure and temperature shock waves within all the three subdomains. The wave propagates radially forward

in the target, backwards in the projectile, and outwards from the point of impact in the fluid. However, due to the difference in magnitudes of pressure between the solid and fluid subdomains, only the variations in the projectile and target is visible in Fig (4). The high temperature and pressure in the fluid causes the argon to ionize, and form a pocket of plasma.

At $t = 0.625 \mu\text{s}$ the projectile has displaced the target material, and a crater has begun to form. The high pressure region behind the rim of the crater causes the target material to accelerate outwards at approximately 5 km/s (V_0). The pocket of plasma has expanded, and is divided into an inner and outer region by the tip of the SLG ejecta. The ejecta accelerates the fluid in the outer region and it reaches velocities of ~ 7 km/s, whereas the fluid in the inner region has velocity magnitudes of ~ 1 km/s. The remnants of the bow shock can still be seen at this time instance. However, the magnitudes of the state variables behind the bow shock are much smaller in comparison to the magnitudes behind the impact generated shock waves; as such the effects of the bow shock on dynamics of the impact are negligible. The temperature behind the shock wave is high in both solids and argon, however, due to the fluid's low density and specific heat the temperature is several orders of magnitude higher.

As time progresses, the shock waves expand further and the energy density behind them decreases. This process can be clearly seen in the snapshots at $t = 2.5 \mu\text{s}$ and $5 \mu\text{s}$. The ionized plasma which was pushed by the ejecta into the outer region, has dissipated significantly faster than in the inner region, as the average charge is much higher within the crater. The pressure wave expands within the target and eventually hits the back wall and causes it to deform radially outwards, and then reflects backwards. The reflected wave destructively interferes with the incident wave, and causes the magnitude of the pressure to fall.

For this representative case ($V_0 = 5$ km/s), the time history of pressure and temperature at the virtual probe (initially) within SLG are shown in Fig. 5. The location of this probe is marked in Fig. 1(B). The probe is fixed in space during the impact process, and crossed by the tantalum-SLG interface at $1.225 \mu\text{s}$. The time intervals in which the probe is located within SLG and tantalum are shaded in light blue and light red colors in Fig. 5. As the shock wave reaches the probe location, both pressure and temperature increase drastically. They keep increasing until the leading edge of the tantalum projectile reaches the probe. Afterwards, both quantities decrease, as the initial forward propagating shock wave propagates and dissipates. A secondary peak is seen in the pressure time history at $t = 4.5 \mu\text{s}$, whereas the temperature does not rise significantly at that time. This occurs as the backward propagating shock wave, which was formed in the projectile at the instance of impact, reaches the probe. The peak pressure and temperature at this probe location are found to be approximately 46 GPa and 3500 K, respectively.

Additional simulations are performed with impact velocity $V_0 = 3$ km/s, 4 km/s, and 6 km/s. In each simulation, the global maximum (i.e. in both space and time) pressure and temperature within SLG are extracted. As expected, these values are achieved at the initial impact point. These peak values are plotted in Fig. 6, in comparison with the experimental results for fused

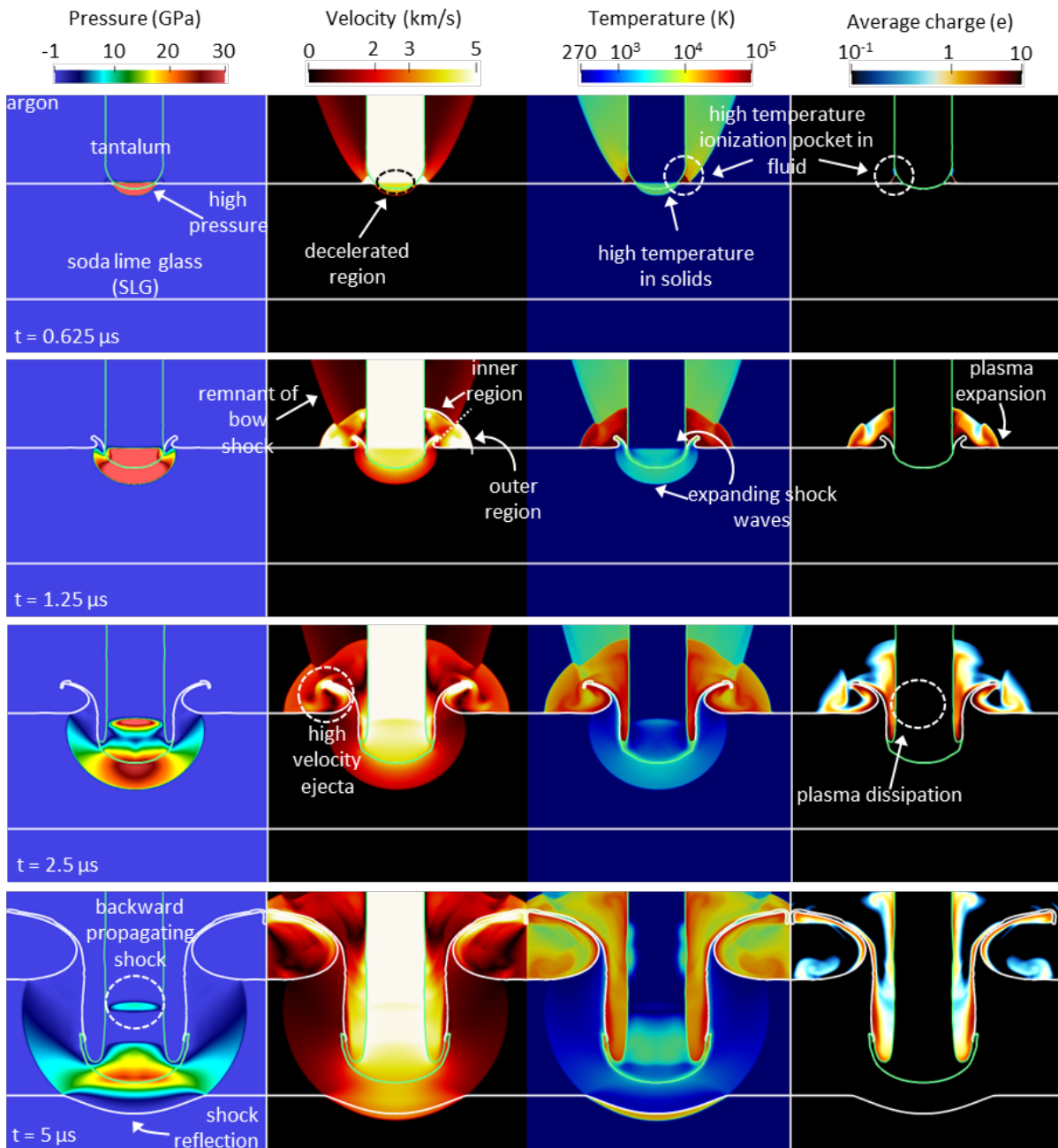


FIGURE 4: SOLUTION SNAPSHOTS OBTAINED FROM A REPRESENTATIVE IMPACT SIMULATION ($V_0 = 5$ km/s).

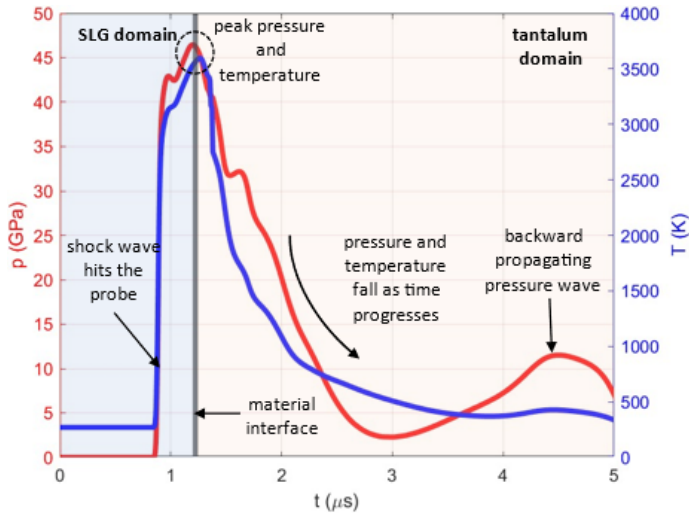


FIGURE 5: TIME HISTORY OF PRESSURE AND TEMPERATURE AT PROBE LOCATION FOR $V_0 = 5$ km/s

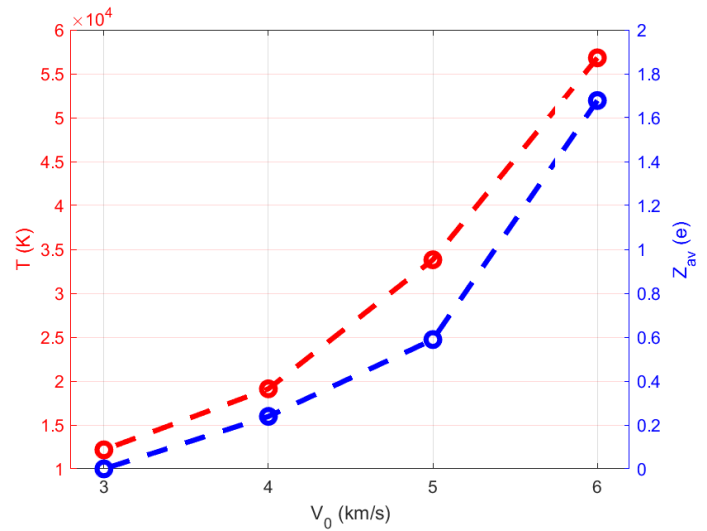


FIGURE 7: MAXIMUM VALUES OF TEMPERATURE (T) AND MEAN CHARGE NUMBER (Z_{av}) CAPTURED BY THE VIRTUAL PROBE WITHIN THE AMBIENT ARGON GAS.

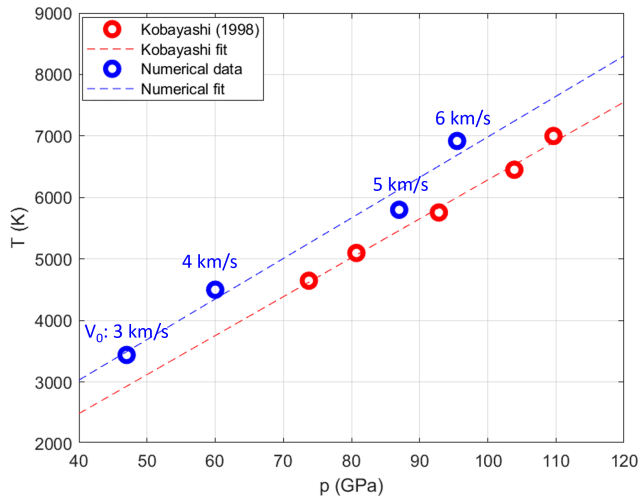


FIGURE 6: SHOCK TEMPERATURE VS. SHOCK PRESSURE VALUES PLOTTED AGAINST DATA PRESENTED BY KOBAYASHI *ET AL.* [6]

quartz presented by Kobayashi *et al.* [6], for a similar range of impact velocities. The computational and experimental results agree reasonably well with each other. The slopes of the linear fit of the data differ by less than 4%. There is some discrepancy in the intercepts of the linear fits, which may be attributed partial to the modeling error due to the different compositions of fused quartz and Starphire SLG.

Another virtual probe is placed within the ambient argon gas, 12 mm from the central axis and 5 mm above the front surface of the SLG target (Fig. 3(B)). Figure 7 shows the maximum values of temperature and mean charge number obtained at this probe location. As expected, as impact velocity increases, both quantities increase accordingly. Comparing this figure with Figs. 5 and 6 shows that the temperature in the ambient gas is significantly higher than that in the solid materials. This is not surprising as temperature is a measure of internal energy per unit mass, and

the mass density of gas is much lower than that of the solids. Therefore, although the fraction of impact energy (i.e. kinetic energy carried by the projectile) transferred to the surrounding gas is small compared to that shared between the solid projectile and target, it is enough to cause dramatic temperature increase in the gas. The high temperature causes argon gas to ionize. Figure 7 shows that at the probe location, ionization is significant for impact velocities higher than 4 kms.

4. CONCLUSIONS

This paper presents a new computational model of hypervelocity impact that accounts for the dynamics, thermodynamics, and ionization of the ambient fluid (gas), as well as the interaction of the fluid flow with the solid projectile and target. The main features of this model include (1) the solution of two level set equations to track three sharp, complex material interfaces, (2) the construction and solution of exact, one-dimensional bimaterial Riemann problems to enforce interface conditions (a method known as “FIVER”), and (3) the solution of Saha equations to predict ionization and plasma density within the ambient fluid. The model is applied to simulate the impact of tantalum projectiles on soda lime glass (SLG) in an argon gas environment, at impact velocities between 3 and 6 km/s. The predicted maximum temperature and pressure within SLG agree reasonably well with published experimental data for a similar material (fused quartz). The temperature in the surrounding gas is found to be significantly higher (by 1 ~ 2 orders of magnitude) than that in the solid materials. This indicates that for impact events that occur in a fluid environment, the fluid may have a substantial effect on the generation of plasma and the emission of electromagnetic waves. For the test case simulated in this paper, ionization of argon is observed at impact velocities above 4 km/s.

ACKNOWLEDGMENT

S.T.I, W.M., and K.W. gratefully acknowledge the support of the Office of Naval Research (ONR) under Award N00014-19-1-

2102. J.G.M. gratefully acknowledges the support of the ONR under award N00014-21-WX01554.

REFERENCES

- [1] Zukas, Jonas A. *High velocity impact dynamics*. Wiley (1990).
- [2] Cour-Palais, Burton G. “Hypervelocity impact in metals, glass and composites.” *International Journal of Impact Engineering* Vol. 5 (1987): pp. 221–237. DOI [10.1016/0734-743x\(87\)90040-6](https://doi.org/10.1016/0734-743x(87)90040-6).
- [3] Li, B, Kidane, A, Ravichandran, G and Ortiz, M. “Verification and validation of the Optimal Transportation Mesh-free (OTM) simulation of terminal ballistics.” *International Journal of Impact Engineering* Vol. 42 (2012): pp. 25–36.
- [4] Birnbaum, Andrew J., Steuben, John C., Iliopoulos, Athanasios P. and Michopoulos, John G. “Simulating hypervelocity impact and material failure in Glass.” *Volume 1B: 38th Computers and Information in Engineering Conference* DOI [10.1115/detc2018-85948](https://doi.org/10.1115/detc2018-85948).
- [5] Barsoum, Roshdy G. “Shockwave compression physics of condensed matter lattice Boltzmann method with application to glass under hypervelocity impact.” (2019).
- [6] Kobayashi, T, Sekine, T, Fat’yanov, OV, Takazawa, E and Zhu, QY. “Radiation temperatures of soda-lime glass in its shock-compressed liquid state.” *Journal of applied physics* Vol. 83 No. 3 (1998): pp. 1711–1716.
- [7] Friichtenicht, Joseph Fred and Slattery, John Charles. “Ionization associated with hypervelocity impact.” Technical report no. 1963.
- [8] Ratcliff, Paul R., Burchell, Mark J., Cole, Mike J., Murphy, Tom W. and Alladfadi, Firooz. “Experimental measurements of hypervelocity impact plasma yield and Energetics.” *International Journal of Impact Engineering* Vol. 20 No. 6-10 (1997): p. 663–674. DOI [10.1016/s0734-743x\(97\)87453-2](https://doi.org/10.1016/s0734-743x(97)87453-2).
- [9] Lee, Nicolas, Close, Sigrid, Goel, Ashish, Lauben, David, Linscott, Ivan, Johnson, Theresa, Strauss, David, Bugiel, Sebastian, Mocker, Anna, Srama, Ralf and et al. “Theory and experiments characterizing hypervelocity impact plasmas on biased spacecraft materials.” *Physics of Plasmas* Vol. 20 No. 3 (2013): p. 032901. DOI [10.1063/1.4794331](https://doi.org/10.1063/1.4794331).
- [10] Fletcher, Alex, Close, Sigrid and Mathias, Donovan. “Simulating plasma production from hypervelocity impacts.” *Physics of Plasmas* Vol. 22 No. 9 (2015): p. 093504. DOI [10.1063/1.4930281](https://doi.org/10.1063/1.4930281).
- [11] Song, Weidong, Li, Jianqiao and Ning, Jianguo. “Characteristics of plasma generated by hypervelocity impact.” *Physics of Plasmas* Vol. 20 No. 9 (2013): p. 093501. DOI [10.1063/1.4819829](https://doi.org/10.1063/1.4819829).
- [12] Li, Jianqiao, Song, Weidong and Ning, Jianguo. “Theoretical and numerical predictions of Hypervelocity Impact-generated plasma.” *Physics of Plasmas* Vol. 21 No. 8 (2014): p. 082112. DOI [10.1063/1.4893310](https://doi.org/10.1063/1.4893310).
- [13] Fletcher, Alex C. and Close, Sigrid. “Particle-in-cell simulations of an RF emission mechanism associated with Hypervelocity Impact Plasmas.” *Physics of Plasmas* Vol. 24 No. 5 (2017): p. 053102. DOI [10.1063/1.4980833](https://doi.org/10.1063/1.4980833).
- [14] Farhat, Charbel, Gerbeau, Jean-Frédéric and Rallu, Arthur. “Fiver: A finite volume method based on exact two-phase Riemann problems and sparse grids for multi-material flows with large density jumps.” *Journal of Computational Physics* Vol. 231 No. 19 (2012): p. 6360–6379. DOI [10.1016/j.jcp.2012.05.026](https://doi.org/10.1016/j.jcp.2012.05.026).
- [15] Wang, K. G., Lea, P. and Farhat, C. “A computational framework for the simulation of high-speed multi-material fluid-structure interaction problems with dynamic fracture.” *International Journal for Numerical Methods in Engineering* Vol. 104 No. 7 (2015): p. 585–623. DOI [10.1002/nme.4873](https://doi.org/10.1002/nme.4873).
- [16] Main, Alex, Zeng, Xianyi, Avery, Philip and Farhat, Charbel. “An enhanced fiver method for multi-material flow problems with second-order Convergence Rate.” *Journal of Computational Physics* Vol. 329 (2017): p. 141–172. DOI [10.1016/j.jcp.2016.10.028](https://doi.org/10.1016/j.jcp.2016.10.028).
- [17] Farhat, C., Wang, K.G., Main, A., Kyriakides, S., Lee, L.-H., Ravi-Chandar, K. and Belytschko, T. “Dynamic implosion of underwater cylindrical shells: Experiments and computations.” *International Journal of Solids and Structures* Vol. 50 No. 19 (2013): p. 2943–2961. DOI [10.1016/j.ijsostr.2013.05.006](https://doi.org/10.1016/j.ijsostr.2013.05.006).
- [18] Wang, Kevin G. “Multiphase fluid-solid coupled analysis of shock-bubble-Stone Interaction in Shockwave Lithotripsy.” *International Journal for Numerical Methods in Biomedical Engineering* Vol. 33 No. 10. DOI [10.1002/cnm.2855](https://doi.org/10.1002/cnm.2855).
- [19] Cao, Shunxiang, Zhang, Ying, Liao, Defei, Zhong, Pei and Wang, Kevin G. “Shock-induced damage and dynamic fracture in cylindrical bodies submerged in liquid.” *International journal of solids and structures* Vol. 169 (2019): pp. 55–71.
- [20] Cao, S, Wang, G, Coutier-Delgosha, O and Wang, K. “Shock-induced bubble collapse near solid materials: Effect of acoustic impedance.” *Journal of Fluid Mechanics* Vol. 907.
- [21] Xiang, Gaoming, Ma, Xiaojian, Liang, Cosima, Yu, Hongyang, Liao, Defei, Sankin, Georgy, Cao, Shunxiang, Wang, Kevin and Zhong, Pei. “Variations of stress field and stone fracture produced at different lateral locations in a shockwave lithotripter field.” *The Journal of the Acoustical Society of America* Vol. 150 No. 2 (2021): p. 1013–1029. DOI [10.1121/10.0005823](https://doi.org/10.1121/10.0005823).
- [22] Ma, Wentao, Zhao, Xuning, Gilbert, Christine and Wang, Kevin. “Computational analysis of bubble–structure interactions in near-field underwater explosion.” *International Journal of Solids and Structures* Vol. 242 (2022): p. 111527.
- [23] Chen, Francis F. *Introduction to plasma physics and Controlled Fusion*. Springer (2018).
- [24] Monroe, Karina A. “Time-Resolved Fractoluminescence Characterization in Soda-Lime Glass Via Near Hypervelocity Kinetic Impact Fast Fracture.” Master’s Thesis, Monterey, CA; Naval Postgraduate School. 2021.
- [25] Razorenov, Sergey V, Garkushin, Gennady, Kanel, Gennady I and Ignatova, Olga Nikolaevna. “The spall strength and Hugoniot elastic limit of tantalum with various grain size.” *AIP Conference Proceedings*, Vol. 1426. 1: pp. 991–994. 2012. American Institute of Physics.

- [26] “AERO-F source code.” (2020). URL <https://bitbucket.org/frg/aero-f/src/master/>.
- [27] “M2C source code.” (2022). URL <https://github.com/kevinwgy/m2c>.
- [28] Mitchell, AC and Nellis, WJ. “Shock compression of aluminum, copper, and tantalum.” *Journal of Applied Physics* Vol. 52 No. 5 (1981): pp. 3363–3374.
- [29] Russell, Alan and Lee, Kok Loong. *Structure-property relations in nonferrous metals*. John Wiley & Sons (2005).
- [30] Katahara, KW, Manghnani, MH and Fisher, ES. “Pressure derivatives of the elastic moduli of BCC Ti-V-Cr, Nb-Mo and Ta-W alloys.” *Journal of Physics F: Metal Physics* Vol. 9 No. 5 (1979): p. 773.
- [31] Huang, J and Gupta, PK. “Temperature dependence of the isostructural heat capacity of a soda lime silicate glass.” *Journal of non-crystalline solids* Vol. 139 (1992): pp. 239–247.
- [32] Robinson, Allen C. “The Mie-Gruneisen Power Equation of State.” Technical report no. Sandia National Lab.(SNL-NM), Albuquerque, NM (United States). 2019.
- [33] Saurel, Richard and Abgrall, Rémi. “A simple method for compressible multifluid flows.” *SIAM Journal on Scientific Computing* Vol. 21 No. 3 (1999): pp. 1115–1145.
- [34] “Starphire Technical Product Data.” Technical Report No. 1.855.887.6457 / 1.855.VTRO.GLS. Vitro Architectural Glass, Pittsburgh, PA. 2020.
- [35] Grady, Dennis E and Chhabildas, LC. “Shock-wave properties of soda-lime glass.” Technical report no. Sandia National Lab.(SNL-NM), Albuquerque, NM (United States). 1996.
- [36] Osher, Stanley and Fedkiw, Ronald P. *Level set methods and dynamic implicit surfaces*. Springer (2009).
- [37] Zaghoul, Mofreh R. “Reduced formulation and efficient algorithm for the determination of equilibrium composition and partition functions of ideal and nonideal complex plasma mixtures.” *Physical Review E* Vol. 69 No. 2. DOI [10.1103/physreve.69.026702](https://doi.org/10.1103/physreve.69.026702).
- [38] Martin, William, Fuhr, Jeffrey, Kelleher, Daniel, Musgrove, Arlene, Sugar, J, Wiese, Wolfgang, Mohr, Peter and Olsen, Karen. “NIST Atomic Spectra Database (version 2.0) (1999).” (1999).
- [39] Alefeld, GE, Potra, Florian A and Shi, Yixun. “Algorithm 748: Enclosing zeros of continuous functions.” *ACM Transactions on Mathematical Software (TOMS)* Vol. 21 No. 3 (1995): pp. 327–344.